Seasoning of plasma etching reactors: Ion energy distributions to walls and real-time and run-to-run control strategies

Ankur Agarwal[a)]
Department of Chemical and Biomolecular Engineering, University of Illinois, 600 South Mathews Avenue, Urbana, Illinois 61801

Mark J. Kushner[b)]
Department of Electrical and Computer Engineering, Iowa State University, 104 Marston Hall, Ames, Iowa 50011

(Received 4 January 2008; accepted 25 March 2008; published 25 April 2008)

Wafer-to-wafer process reproducibility during plasma etching often depends on the conditioning of the inside surfaces of the reactor. Passivation of reactor surfaces by plasma generated species, often called seasoning, can change the reactive sticking coefficients of radicals, thereby changing the composition of the radical and ion fluxes to the wafer. Ion bombardment of the walls may influence these processes through activation of surface sites or sputtering, and so the spatial variation of ion energies on the walls is important. These seasoning processes may occur during a single etching process or on a wafer-to-wafer basis. The seasoning of plasma etching reactors will be discussed using results from a computational investigation of *p*-Si etching in chlorine plasmas. The transport of etch products, passivation of walls, and sputtered products from walls are accounted for, as well as differentiating the ion energy distributions to different surfaces. A real-time, closed-loop control of etch rate to counter the effects of seasoning was achieved using the bias voltage as an actuator.
© *2008 American Vacuum Society.* [DOI: 10.1116/1.2909966]

I. INTRODUCTION

Wafer-to-wafer reproducibility during plasma etching of semiconductor devices continues to remain a challenge.[1,2] To ensure that the critical dimensions of devices are consistently reproduced, a uniform plasma with the same ion density, electron temperature, and fluxes to the wafer must be maintained for each wafer. Many etch processes employ low pressure (less than tens of milliTorr) plasmas where the mean-free-paths of radicals and ions may be comparable to the reactor dimensions. These long mean-free-paths increase the importance of plasma-surface interactions on nonwafer surfaces.[3] The use of high plasma density systems having high processing rates increases the likelihood of buildup of etch products in the volume of the process chamber which can interact with and deposit on wafer and nonwafer surfaces. When operating at constant pressure, the etch products can displace the desired reactant species and so reduce their fluxes to the wafer.[4,5]

Etch products can alter the gas phase composition of both ions and neutrals, and the electron temperature, in at least two ways. The first is by their being gas phase collision partners which consume discharge power and provide new collision partners for the feedstock gases. The second is by reactions with wafer and walls surfaces which may change reactive sticking coefficients for other species.[6,7] For example, Zhou *et al.*[7] investigated the effects of wall conditions (temperature and cleanliness) on gas phase chemistry and etching rates of Si and SiO_2 in a CF_4 plasma. They found that if the walls are not initially clean, CF_2 and CF_3 densities increase with increasing wall temperature as much as 80% compared to densities in a reactor with clean walls. The etch rate of SiO_2 was fairly independent of the wall temperature or cleanliness, while the etch rate of Si decreased with wall temperature and as deposits built up on the walls. Ullal *et al.*[8] observed a gradual increase in gas phase densities of $SiCl_x$ and Cl and an increase in the total ion flux to the substrate in a Cl_2 inductively coupled plasma in the absence of a Si wafer. These trends were attributed to the coating of the chamber walls with a glassy silicon oxychloride film resulting from sputtering of the quartz window (the only significant source of Si and O). Cleaning the walls with a SF_6 plasma restored the reactor to its original operating conditions.

The gradual deposition of etch products (or feedstock gas fragments) on the surfaces of the plasma chamber can result in the drift of process variables, such as etch rates, etch profiles, selectivity, and uniformity. The change in reactor wall conditions in this manner is often referred to as seasoning of the chamber. A reactor undergoing seasoning during a given etch process may experience a drift in, for example, etch rate. A well seasoned reactor with walls that are fully passivated will have achieved a steady and experience less process drift. For example, Kim *et al.*[9] investigated the consequences of reactor seasoning on the rate and uniformity of etching *p*-Si in an inductively coupled Cl_2 plasma. The maximum etch rate shifted from the center of the wafer in an unseasoned reactor to the edge of the wafer when the walls were fully passivated, in this case with a silicon oxychloride film.

[a)]Present address: Applied Materials, Inc., 974 E. Arques Ave., M/S 81517, Sunnyvale, CA 94085; electronic mail: ankur_agarwal@amat.com
[b)]Author to whom correspondence should be addressed; electronic mail: mjk@iastate.edu

To eliminate process drift, plasma chambers are often seasoned using a sacrificial wafer prior to processing a production wafer to precoat the walls with the film that would otherwise be deposited during the course of etching the production wafer. When a reactor is properly seasoned, the inner surfaces are passivated to an unchanging state before starting to process the production wafer. Although the ideal situation is to season the reactor with the same process as used for the production wafer, other chemistries may be used to speed the seasoning step.[10–13]

Self-cleaning plasma chemistries provide another alternative. In this mode, feedstock gases provide the dual role of etching the wafer and minimizing the net deposition of etch products on the reactor walls by etching depositions on the wall as well.[10] For example, the deposition of silicon oxychloride films decreases with the addition of CF_4 in the feedstock gases.[11] Although promising, the process does not entirely prevent deposition of coatings on the reactor walls. For example, the deposition of Si-based species may be reduced but the deposition of carbon-based materials may increase. The deposition of these carbon polymer layers can be mitigated with the addition of O_2.

Another strategy is to remove the wall passivation produced by a previous process by plasma cleaning the chamber before beginning the next process. The cleaning step resets the chamber to known conditions prior to etching the production wafer. Although effective, this strategy reduces the throughput of production wafers and may not eliminate transients due to seasoning that may occur during the subsequent etch process. For silicon etching processes, the reactor dry cleans can be achieved using fluorine-based chemistries, typically SF_6/O_2.[12] However, the use of fluorine-based plasmas with, for example, Al_2O_3 walls may result in formation of and accumulation of nonvolatile AlF_x on reactor walls. This accumulation can itself produce process drifts.[13]

To eliminate the costs of cleaning of reactors after each wafer to address wafer-to-wafer seasoning and drift, feedback control with *in situ* diagnostics have been proposed to monitor plasma properties and take corrective actions to restore a desired performance level.[14–16] For example, feedback schemes have been applied to control *p*-Si etch rates in Cl_2 plasmas.[17–20] The choice of actuators and sensors are governed by experimentally measurable quantities. For example, Donnelly[21] showed that optical emission actinometry can be used to determine absolute chlorine densities when *p*-Si is etched in a Cl_2 helicon resonator produced plasma. Garvin *et al.*[22] developed a microwave cavity resonance sensor to measure plasma density. Direct measurements of the etch rate can be made with surface characterizing optical techniques such as spectroscopic ellipsometry (SE), although *p*-Si is a difficult film to characterize with SE because of $\sim 10-20$ nm level surface roughness.[23] Sarfaty *et al.*[24] used a two-color laser interferometry to determine the etch rate and etch selectivity of unpatterned *p*-Si and SiO_2 films in a Cl_2 plasma.

Easily implementable actuators for control of plasma processes include power to the wafer or to the antenna, gas flow rate, and gas pressure. For example, Choe *et al.*[18] showed that the silicon etch rate is controlled by the ion current to the wafer in a Cl_2 plasma. Patrick *et al.*[19] showed that the radio frequency (rf) peak voltage and sheath voltage have similar correlations. Lin *et al.*[20] implemented a proportional-integral controller using rf power to the wafer and antenna as actuators to maintain a constant ion current and rf voltage (control variables). Sarfaty *et al.*[17] implemented a proportional integral derivative controller to maintain etch rate by means of rf power to the wafer in a magnetically confined inductively coupled plasma tool.

Although many experiments have investigated wafer-plasma interactions in the context of chamber seasoning, few models have addressed the long term drift of plasma and etch properties resulting from wall contamination and seasoning.[25–28] In this article, we report on a computational investigation of the consequences of seasoning of chamber surfaces during the Ar/Cl_2 plasma etching of poly-Si in an inductively coupled plasma (ICP) having a quartz window under the antenna. Ion bombardment of the walls may influence the coverage of passivation or production of etch influencing species through activation of surface sites or sputtering of physi- or chemisorbed species. As such, the spatial distributions of ion energies on the walls and their evolution as the chamber seasons were included in the model. The consequences on etch rates, uniformity, and coverage of species on the wafer and reactor surfaces will be discussed.

Two wall reaction mechanisms were investigated. In the first mechanism, the deposition of etch products on the walls is limited to a few monolayers (with etch products not sticking to passivated walls). With this mechanism, reactor seasoning produces a decrease in sticking coefficients for etch products and Cl atoms, which increases their gas phase densities and increases their fluxes to the wafer. Redeposition of the etch products on the wafer produces etch blocks, which reduces etch rates. In the second mechanism, etch products are allowed to buildup multiple layers on the reactor walls while reducing the reactivity of Cl atoms. In this mechanism, etch rates increase with seasoning. We also found that fairly subtle changes in the placement of the coils above the quartz window can have significant effects on the seasoning of the reactor. The height of the coils above the quartz determines the amount of capacitive coupling to the plasma and the ion energies incident onto the quartz. This in turn determines the amount of sputtering of the quartz and the flux of O atoms injected into the plasma. The O atoms are a potential source of etch blocks (e.g., SiOCl) and wall passivation.

We also investigated feedback control schemes to maintain a constant etch rate on both a real-time and run-to-run basis. We assumed the availability of a sensor to directly measure the etch rate and a proportional controller was used to vary the bias voltage to stabilize the rate. We found that such a scheme can stabilize the process during a given process while wafer-to-wafer control is sometimes complicated by the disparity between the fresh state of a newly inserted wafer compared to the condition of the wafer at the end of the prior process.

The models and reactions mechanism used in this investigation are described in Sec. II. Results for seasoning of reactors during etching of p-Si in Ar/Cl_2 plasmas are discussed in Sec. III. The consequences of reactor design on seasoning are discussed in Sec. IV. Closed-loop feedback control strategies to counter drifts in etch rates are described in Sec. V. Concluding remarks are presented in Sec. VI.

II. DESCRIPTION OF THE MODELS

In this section, the models, reaction mechanisms, and control schemes used in this investigation will be discussed.

A. Plasma and surface models

The hybrid plasma equipment model (HPEM) was used to predict the reactor scale plasma characteristics and reactant fluxes to surfaces in the ICP reactor. The HPEM has been previously described and so will only be briefly discussed here.[29,30] The HPEM is a two-dimensional, modular model which addresses gas phase and surface kinetics. Electromagnetic fields, as calculated in the electromagnetics module, are used in the electron energy transport module to obtain electron impact source functions and transport coefficients. This was accomplished by solving the electron energy equation for the average electron energy of bulk electrons, with transport coefficients coming from a solution of Boltzmann's equation, and using a Monte Carlo simulation to follow the trajectories of sheath accelerated secondary electrons. The transport coefficients and source functions are used by the fluid kinetics module (FKM) to solve separate continuity, momentum, and energy equations for each ion and neutral species, while implicitly solving Poisson's equation for the time varying electrostatic potential. The FKM outputs the densities and electrostatic fields which are then transferred to the other modules. This process is iterated until a converged quasisteady state solution is obtained or allowed to evolve for a time dependent solution.

Reaction probabilities for surface chemistry are provided by the surface chemistry module (SCM) which computes the composition of surface resident species using a multilayer surface-site-balance model. The reaction mechanism is unique for each surface in contact with the plasma. The plasma chemistry Monte Carlo module (PCMCM) produces the energy and angular distributions for neutrals and ions striking surfaces in contact with the plasma. The PCMCM launches pseudoparticles representing ions and neutrals based on the electron impact source functions. Using time dependent electric fields from the FKM, their trajectories are integrating while accounting for gas phase collisions. Statistics are collected on the energy and angle of pseudoparticles as they strike surfaces.

The SCM is structurally similar to that described in Ref. 29. The improvement here is the calculation of ion energy dependent reaction probabilities.[31] In the prior work, ion energy distributions were approximated as a function of position based on sheath characteristics. In this work, the ion energy and angular distributions (IEADs) obtained from the PCMCM are used to compute energy dependent reaction probabilities used in the SCM on a material-by-material basis. The probabilities for surface reactions involving energetic species (either ions or hot neutrals) are given by[31]

$$p(E) = p_o \frac{E^m - E_t^m}{E_r^m - E_t^m}, \qquad (1)$$

where $p(E)$ is the reaction probability for a particle with energy E, E_t is the threshold energy of the process, E_r is a reference energy, and p_o is the reaction probability at the reference energy. Typically, $m=0.5$ for sputtering or ion activated etching, and that value was used here. The probability for a given reaction along the surface is then given by

$$p(x) = \frac{\int f_i(E,x)p(E)dE}{\int f_i(E,x)dE}, \qquad (2)$$

where $f_i(E,x)$ is the ion energy distribution function as a function of position on the wall. The PCMCM is executed periodically during the simulation to provide $f_i(E,x)$ which captures changes in the fluxes (composition and energy) that may affect surface reaction probabilities.

B. Surface reaction mechanism

The seasoning of reactors during etching of p-Si using chlorine plasmas was investigated. The reaction mechanism for Ar/Cl_2 mixtures was discussed and validated in Ref. 32. The p-Si etching surface mechanism and species we used are listed in Table I and are based on the works of Cheng *et al.*[33] and Meeks and Shon.[34] They are discussed in detail in Ref. 35. The mechanism is schematically shown in Fig. 1(a). Etching of the Si wafer takes place by successively chlorinating the polysilicon surface, forming $SiCl_n(s)$ [$SiCl(s)$ followed by $SiCl_2(s)$ and $SiCl_3(s)$], where (s) denotes a surface species. Following passivation, the removal of the $SiCl_n$ etch product then occurs through ion activation. To simplify the gas phase reaction mechanism etch products released into the gas phase were limited to $SiCl_2$ and $SiCl_4$. The $SiCl_2$ etch products in the bulk plasma can redeposit on the wafer forming $Si_2Cl_y(s)$ species which are treated as etch blocks. The etch blocks must be removed by ion bombardment to allow etching of the underlying Si to proceed. The reaction mechanism is summarized as

$$Cl + Si(s) \rightarrow SiCl(s), \quad p=0.99, \qquad (3)$$

$$Cl + SiCl_n(s) \rightarrow SiCl_{n+1}(s), \quad p=0.2, \qquad (4)$$

$$M^+ + SiCl_n(s) \rightarrow SiCl_n + M, \quad p=0.6, \qquad (5)$$

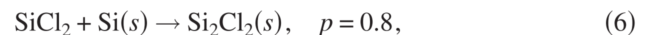

$$SiCl_2 + Si(s) \rightarrow Si_2Cl_2(s), \quad p=0.8, \qquad (6)$$

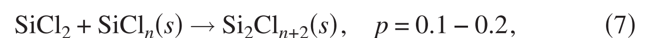

$$SiCl_2 + SiCl_n(s) \rightarrow Si_2Cl_{n+2}(s), \quad p=0.1-0.2, \qquad (7)$$

TABLE I. Surface reaction mechanism for Si etching in Ar/Cl_2 plasmas.

Species	M gas phase species	
M(s) surface site		
W(s) reactor wall surface site		

Reaction[a–c]	Probability	Footnote
Wafer: Formation of passivation layer:		
$Cl+Si(s) \rightarrow SiCl(s)$	0.99	
$Cl+SiCl(s) \rightarrow SiCl_2(s)$	0.2	
$Cl+SiCl_2(s) \rightarrow SiCl_3(s)$	0.15	
$Cl^*+Si(s) \rightarrow SiCl(s)$	0.6	
$Cl^++Si(s) \rightarrow SiCl(s)$	0.4	
Wafer: Formation of etch blocks:		
$SiCl_2+Si(s) \rightarrow Si_2Cl_2(s)$	0.9	
$SiCl_2+SiCl(s) \rightarrow Si_2Cl_3(s)$	0.9	
$SiCl_2+SiCl_2(s) \rightarrow Si_2Cl_4(s)$	0.9	
Wafer: Consumption of passivation etch blocks:		
$Cl+SiCl_2(s) \rightarrow SiCl(s)+Cl_2$	0.02	
$Cl+SiCl_3(s) \rightarrow SiCl_4+Si(s)$	0.001	
$Cl+SiCl_3(s) \rightarrow SiCl_2(s)+Cl_2$	0.08	
$Cl+Si_2Cl_2(s) \rightarrow SiCl(s)+SiCl_2$	0.008	
$Cl+Si_2Cl_3(s) \rightarrow SiCl(s)+SiCl_2+Cl$	0.008	
$Cl+Si_2Cl_4(s) \rightarrow SiCl_2(s)+SiCl_2+Cl$	0.008	
$Cl^*+SiCl(s) \rightarrow SiCl_2+Si(s)$	0.25	
$Cl^*+SiCl_2(s) \rightarrow SiCl_2+Cl+Si(s)$	0.5	
$Cl^*+SiCl_3(s) \rightarrow SiCl_4+Si(s)$	0.5	
$Cl^*+Si_2Cl_2(s) \rightarrow Si(s)+SiCl_2+Cl$	0.8	
$Cl^*+Si_2Cl_3(s) \rightarrow SiCl(s)+SiCl_2+Cl$	0.9	
$Cl^*+Si_2Cl_4(s) \rightarrow SiCl_2(s)+SiCl_2+Cl$	0.9	
$Cl^++SiCl(s) \rightarrow SiCl_2+Si(s)$	0.3	d
$Cl^++SiCl_2(s) \rightarrow SiCl_2+Cl+Si(s)$	0.6	d
$Cl^++SiCl_3(s) \rightarrow SiCl_4+Si(s)$	0.6	d
$Cl^++Si_2Cl_2(s) \rightarrow Si(s)+SiCl_2+Cl$	0.9	d
$Cl^++Si_2Cl_3(s) \rightarrow SiCl(s)+SiCl_2+Cl$	0.99	d
$Cl^++Si_2Cl_4(s) \rightarrow SiCl_2(s)+SiCl_2+Cl$	0.99	d
$Cl_2^++Si(s) \rightarrow SiCl_2+Si(s)$	0.002	d
$Cl_2^++SiCl(s) \rightarrow SiCl_2+Cl+Si(s)$	0.25	d
$Cl_2^++SiCl_2(s) \rightarrow SiCl_2+Cl_2+Si(s)$	0.6	d
$Cl_2^++SiCl_3(s) \rightarrow SiCl_4+Cl+Si(s)$	0.6	d
$Cl_2^++Si_2Cl_2(s) \rightarrow Si(s)+SiCl_2+Cl_2$	0.9	d
$Cl_2^++Si_2Cl_3(s) \rightarrow SiCl(s)+SiCl_2+Cl_2$	0.99	d
$Cl_2^++Si_2Cl_4(s) \rightarrow SiCl_2(s)+SiCl_2+Cl_2$	0.99	d
$Ar^*+SiCl_2(s) \rightarrow SiCl_2+Ar+Si(s)$	0.3	
$Ar^*+Si_2Cl_2(s) \rightarrow Si(s)+SiCl_2+Ar$	0.8	
$Ar^*+Si_2Cl_3(s) \rightarrow SiCl(s)+SiCl_2+Ar$	0.9	
$Ar^*+Si_2Cl_4(s) \rightarrow SiCl_2(s)+SiCl_2+Ar$	0.9	
$Ar^++SiCl_2(s) \rightarrow SiCl_2+Ar+Si(s)$	0.4	d
$Ar^++SiCl_2(s) \rightarrow SiCl_2(s)+Ar$	0.6	d
$Ar^++Si_2Cl_2(s) \rightarrow Si(s)+SiCl_2+Ar$	0.9	d
$Ar^++Si_2Cl_3(s) \rightarrow SiCl(s)+SiCl_2+Ar$	0.99	d
$Ar^++Si_2Cl_4(s) \rightarrow SiCl_2(s)+SiCl_2+Ar$	0.99	d
$SiCl_2^++SiCl_2(s) \rightarrow SiCl_2+SiCl_2+Si(s)$	0.6	d
$SiCl_2^++Si_2Cl_2(s) \rightarrow Si(s)+SiCl_2+SiCl_2$	0.9	d
$SiCl_2^++Si_2Cl_3(s) \rightarrow SiCl(s)+SiCl_2+SiCl_2$	0.99	d
$SiCl_2^++Si_2Cl_4(s) \rightarrow SiCl_2(s)+SiCl_2+SiCl_2$	0.99	d
Non-wafer surfaces:		
$Cl+W(s) \rightarrow Cl(s)$	0.02	
$Cl+Cl(s) \rightarrow W(s)+Cl_2$	0.02	
$Cl^*+W(s) \rightarrow Cl(s)$	0.06	
$Cl+SiCl_2(s) \rightarrow SiCl_2(s)+Cl$	1	
$Cl^*+Cl(s) \rightarrow W(s)+Cl_2$	0.16	
$Cl^*+SiCl_2(s) \rightarrow W(s)+SiCl_2+Cl$	0.04	
$Cl^++Cl(s) \rightarrow W(s)+Cl_2$	0.8	
$Cl^++SiCl_2(s) \rightarrow W(s)+SiCl_2+Cl$	0.5	d
$Cl^++SiCl_2(s) \rightarrow SiCl(s)+Cl_2$	0.1	e
$Cl_2^++Cl(s) \rightarrow W(s)+Cl_2+Cl$	0.8	
$Cl_2^++SiCl_2(s) \rightarrow W(s)+SiCl_2+Cl_2$	0.84	d
$Cl_2^++SiCl_2(s) \rightarrow SiCl(s)+Cl_2+Cl$	0.1	e
$Ar^*+Cl(s) \rightarrow W(s)+Cl+Ar$	0.06	
$Ar^*+SiCl_2(s) \rightarrow W(s)+SiCl_2+Ar$	0.04	
$Ar^++Cl(s) \rightarrow W(s)+Cl+Ar$	0.4	
$Ar^++SiCl_2(s) \rightarrow W(s)+SiCl_2+Ar$	0.8	d
$Ar^++SiCl_2(s) \rightarrow SiCl(s)+Cl+Ar$	0.1	e
$SiCl_2+W(s) \rightarrow SiCl_2(s)$	0.2	
$SiCl_2+Cl(s) \rightarrow Cl(s)+SiCl_2$	1	
$SiCl_2+SiCl_2(s) \rightarrow SiCl_2(s)+SiCl_2$	1	
$SiCl_2^++W(s) \rightarrow W(s)+SiCl_2$	1	
$SiCl_2^++Cl(s) \rightarrow W(s)+SiCl_2+Cl$	0.8	d
$SiCl_2^++SiCl_2(s) \rightarrow W(s)+SiCl_2+SiCl_2$	0.04	d
$SiCl_2^++SiCl_2(s) \rightarrow SiCl(s)+SiCl_2+Cl$	0.1	e

[a]Unless specified, all ions neutralize on surfaces, returning as their neutral counterparts.
[b]Gas phase species have units of flux ($cm^{-2}\ s^{-1}$). Surface species have units of fractional coverage.
[c]In reactions with no chemical change, the gas species are reflected off the surface. These reactions are not shown.
[d]See Eq. (1). E_r=150 eV, E_t=20 eV.
[e]See Eq. (1). E_r=150 eV, E_t=30 eV.

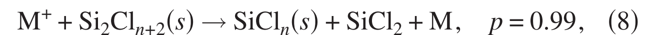

$$M^+ + Si_2Cl_{n+2}(s) \rightarrow SiCl_n(s) + SiCl_2 + M, \quad p = 0.99, \quad (8)$$

where M^+ represents any ion (or hot neutral) and p is the default probability or the probability at the reference energy of 150 eV. Threshold energies for ion processes are 20 eV unless otherwise specified.

The plasma-surface reaction mechanism on nonwafer surfaces is based on the work of Cunge *et al.*[36] It is also summarized in Table I and shown schematically in Fig. 1(a). The etch products can stick to the walls which can then be further sputtered or etched by ions and hot neutrals

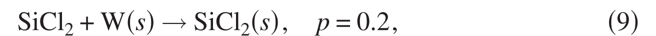

$$SiCl_2 + W(s) \rightarrow SiCl_2(s), \quad p = 0.2, \quad (9)$$

$$SiCl_2 + SiCl_2(s) \rightarrow \text{(no reaction)}, \quad (10)$$

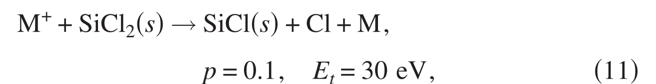

$$M^+ + SiCl_2(s) \rightarrow SiCl(s) + Cl + M, \quad p = 0.1, \quad E_t = 30\ \text{eV}, \quad (11)$$

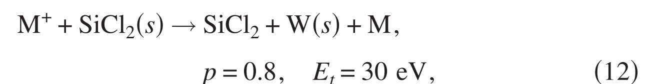

$$M^+ + SiCl_2(s) \rightarrow SiCl_2 + W(s) + M, \quad p = 0.8, \quad E_t = 30\ \text{eV}, \quad (12)$$

where M^+ represents any ion (or hot neutral), W is a native

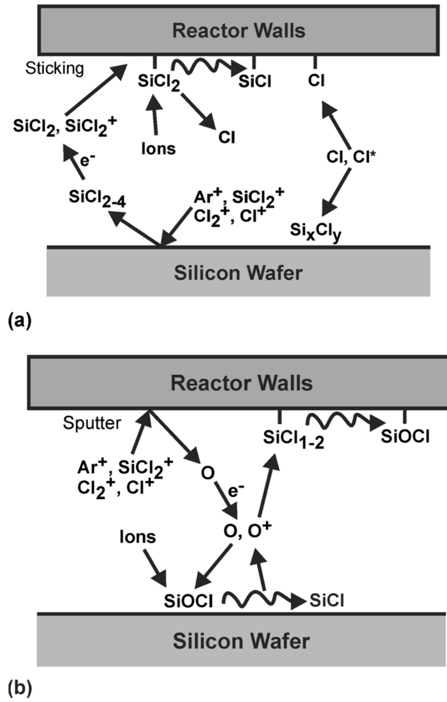

FIG. 1. Schematic of the surface mechanisms for Si etching in an Ar/Cl_2 plasma. (a) Si_xCl_y etch products form etch blocks, Si_2Cl_y, on the wafer. (b) Sputtering of quartz produces oxygen atoms which form etch blocks, SiOCl, on the wafer.

TABLE II. Additional reactions for Si etching in Ar/Cl_2 with oxygen fluxes.

Species:
M gas phase species
M^+ ion
$M(s)$ surface site
$Q(s)$ quartz window surface site

Reaction[a–c]	Probability	Footnote
Oxygen sputtering from quartz window:		
$M^+ + Q(s) + Q(s) + M + O$	1.0	d
Formation of etch blocks:		
$O + SiCl(s) \rightarrow SiOCl(s)$	1.0	
$O + SiCl_2(s) \rightarrow SiOCl(s)$	1.0	
$O + SiCl_3(s) \rightarrow SiOCl(s)$	1.0	
$O + Si_2Cl_2(s) \rightarrow SiOCl(s)$	1.0	
$O + Si_2Cl_3(s) \rightarrow SiOCl(s)$	1.0	
$O + Si_2Cl_4(s) \rightarrow SiOCl(s)$	1.0	
Removal of etch blocks:		
$M^+ + SiOCl(s) \rightarrow SiCl(s) + M + O$	1.0	e

[a]Unless specified, all ions neutralize on surfaces, returning as their neutral counterparts.
[b]Gas phase species have units of flux ($cm^{-2}\ s^{-1}$). Surface species have units of fractional coverage.
[c]In reactions with no chemical change, the gas species are reflected off the surface. These reactions are not shown in the table.
[d]See Eq. (1). $E_r = 150$ eV, $E_t = 50$ eV.
[e]See Eq. (1). $E_r = 150$ eV, $E_t = 60$ eV.

wall surface site, and p is the probability which for ions is at the reference energy of 150 eV. Cl atoms may adsorb onto bare wall sites and abstract adsorbed Cl but are otherwise unreactive with passivated sites

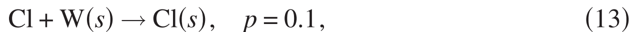

$$Cl + W(s) \rightarrow Cl(s), \quad p = 0.1, \tag{13}$$

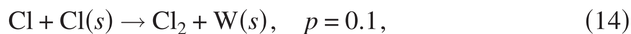

$$Cl + Cl(s) \rightarrow Cl_2 + W(s), \quad p = 0.1, \tag{14}$$

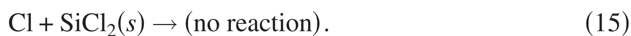

$$Cl + SiCl_2(s) \rightarrow (\text{no reaction}). \tag{15}$$

Two variants of the surface reaction mechanism were investigated. The first, described earlier, essentially allows for a single layer of passivation of etch products on the walls (metal sidewalls and dielectric window). Etch products then do not further stick to the passivation, as in Eq. (10). In the second variant, etch products are allowed to stick to the wall passivation

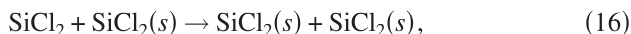

$$SiCl_2 + SiCl_2(s) \rightarrow SiCl_2(s) + SiCl_2(s), \tag{16}$$

thereby building up multiple layers of passivation. In the former variant, the reaction probability of $SiCl_2$ to walls decreases as the reactor is seasoned, as does the reaction probability of Cl. In the latter variant, the reaction probabilities of $SiCl_2$ to walls do not significantly decrease as the reactor is seasoned, where as those for Cl do continue to decrease.

ICP reactors typically have dielectric windows above which the antenna sits and through which the electromagnetic fields enter the plasma. Quartz is a common material for the window. Sputtering of the quartz window by ions is a potential source of oxygen atoms in the plasma which may lead to the formation of silicon oxychloride films.[37–39] We included sputtering of O atoms from the quartz window using the algorithms discussed in Ref. 40. O atoms were sputtered with a threshold energy of 60 eV with a probability of 1.0 at a reference energy of 150 eV.

The surface reaction mechanism including oxygen atoms is schematically shown in Fig. 1(b) and is summarized in Table II. The oxygen species in the gas phase mechanism include ground-state neutral O; electronically excited $O(^1D)$, and the ion O^+. The complete gas phase reaction mechanism involving O atoms is shown in Table I of Ref. 41. Oxygen atoms can adsorb on any Si_xCl_y passivated surface site forming SiOCl which, if on the wafer, is treated as an etch block. The etch block is removed, allowing the etch to proceed, when an oxygen atom is removed from the oxychloride film by energetic ions

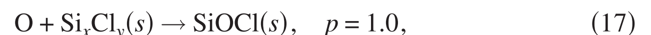

$$O + Si_xCl_y(s) \rightarrow SiOCl(s), \quad p = 1.0, \tag{17}$$

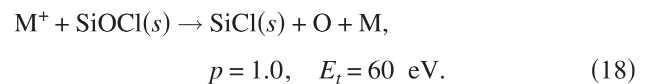

$$M^+ + SiOCl(s) \rightarrow SiCl(s) + O + M, \quad p = 1.0, \quad E_t = 60 \text{ eV}. \tag{18}$$

C. Real time control algorithms

The HPEM has modules which address real-time control (RTC) through the implementation of sensors and actuators.[42] At the desired controller frequency, the execution of the HPEM is paused and the RTC modules are executed.

In the sensor module, models of sensors are implemented which provide the simulated outputs of experimental diagnostics. These sensor outputs are then used as inputs to the controller module which computes changes in settings of actuators to restore the system to a desired operating point. These recommendations are passed to the actuator module which makes adjustments in the settings of process variables, such as pressure, power, or bias voltage.

In this work, a proportional controller was used to compensate for process drifts by varying the bias voltage (the actuator) applied to the substrate. The etch rate (as might be measured by an *in situ* laser interferometer) was used as the sensor.[15] The time between controller actions was chosen to be longer than the equilibration time of the plasma following perturbations to its operating conditions. Therefore, the plasma reaches a quasisteady state between actuator adjustments. Since typical controller frequencies are a few tens of hertz, and the plasma equilibration time (excluding neutral gas flow) is at worst a few to tens of milliseconds, this is a good approximation.

III. SEASONING OF REACTORS DURING ETCHING OF SI IN AN AR/CL_2 PLASMA

The system investigated here is the ICP reactor schematically shown in Fig. 2(a). Inductive power is supplied through a three-turn coil, 16 cm in diameter in contact with 0.8 cm thick quartz window which is 23 cm in diameter. The wafer is on an independently powered substrate, 9 cm below the quartz window. The process conditions are a 15 mTorr Ar/Cl_2=90/10 gas mixture with a flow rate of 25 sccm. The coil delivers 500 W at 10 MHz. Both purely inductive and capacitively coupled configurations of the coil were considered. The amplitude of the 5 MHz rf bias waveform at the electrode will be varied.

A typical computational strategy is as follows. Initial conditions (e.g., plasma density, dissociation fraction) are estimated and the model is executed with only ICP power for 60 μs to achieve a quasisteady state in plasma characteristics. (The effective integration time is actually 10–100 times longer as acceleration techniques are used to speed the convergence of plasma properties.) Silicon etching is then enabled by applying the bias voltage using direct time integration technique (that is, no acceleration) in the SCM. The surface reaction rate coefficients for gas phase species are updated by the SCM every 2 s. The etching of a series of wafers was modeled for a total of 180 s for each wafer. When a new wafer is started the surface of the wafer is initialized to have unprocessed conditions while the reactor walls maintain their seasoned surface coverages.

The densities of all positive ions and the $SiCl_2$ etch product are shown in Fig. 2(b) for a bias voltage of 75 V. Cycle-averaged radical and ion fluxes to the wafer are shown in Fig. 3. The peak ion density is 2.8×10^{11} cm^{-3} and the $SiCl_2$ has a maximum density of 9×10^{11} cm^{-3} near its source at the wafer. The average density of $SiCl_2$ in the bulk plasma of 1.5×10^{11} cm^{-3} results, in part, from passivation of the walls of the reactor which reduces its sticking coefficient. The

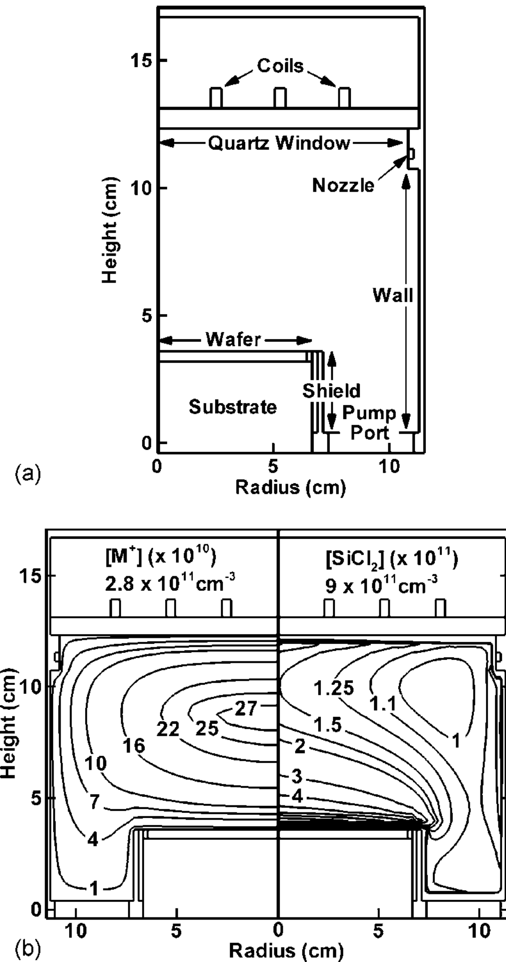

FIG. 2. Schematic of the ICP reactor. (a) Location and orientation of surfaces having unique reaction mechanisms. (b) Total ion density and density of $SiCl_2$ for Ar/Cl_2=90/10, 500 W ICP, 15 mTorr, 100 sccm, and 75 V substrate bias. Silicon etching by chlorine is the only source of $SiCl_2$ in the bulk plasma. Contour labels have units shown in parenthesis and maximum densities are noted in the figure.

$SiCl_2$ redeposits on the wafer which produces process drifts. The Cl and etch product fluxes, on axis, are Cl (0.9×10^{17} cm^{-2} s^{-1}), $SiCl_2$ (6.9×10^{15} cm^{-2} s^{-1}), and $SiCl_4$ (2.5×10^{15} cm^{-2} s^{-1}). The largest fluxes of ions are due to Ar^+ (2.2×10^{16} cm^{-2} s^{-1}) and Cl^+ (2.0×10^{15} cm^{-2} s^{-1}). The fluxes of Cl_2^+ and $SiCl_2^+$ are an order of magnitude lower. The fluxes are center peaked (no attempt was made to optimize the radial uniformity of the fluxes). Since the flux of Cl is essentially uniform across the wafer, spatially dependent etch rates result from the radial dependence of the ion and redeposition fluxes.

The IEADs for all ions averaged over the wafer, the sidewall, and the quartz window [see locations in Fig. 2(a)] without capacitive coupling from the coils are shown in Fig. 4(a). The rf amplitude on the substrate is 75 V and the dc bias is −37 V. The IEAD for the wafer extends from 25 to 160 eV with a two-peak shape characteristic of nearly collisionless transport through a thin sheath. The ion energies extend above the threshold energy for Si etching, with the probability for etching a $SiCl_2(s)$ site being 0.63 at the peak ion

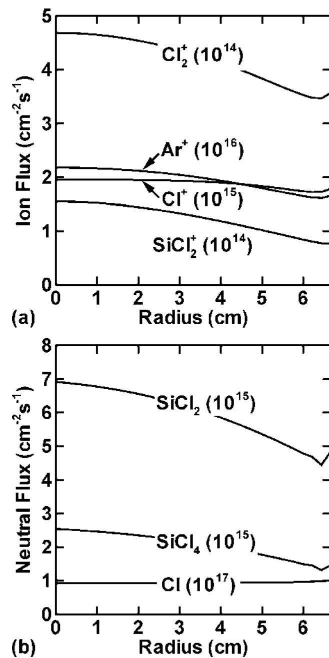

FIG. 3. Fluxes to the wafer as a function of radius (Ar/Cl_2=90/10, 500 W ICP, 15 mTorr, 100 sccm) and 75 V substrate bias. (a) Ion fluxes and (b) neutral fluxes. The scaling values for the fluxes are indicated in the figure. Cl is the major neutral radical flux. Ar^+ and Cl^+ are the dominant ions.

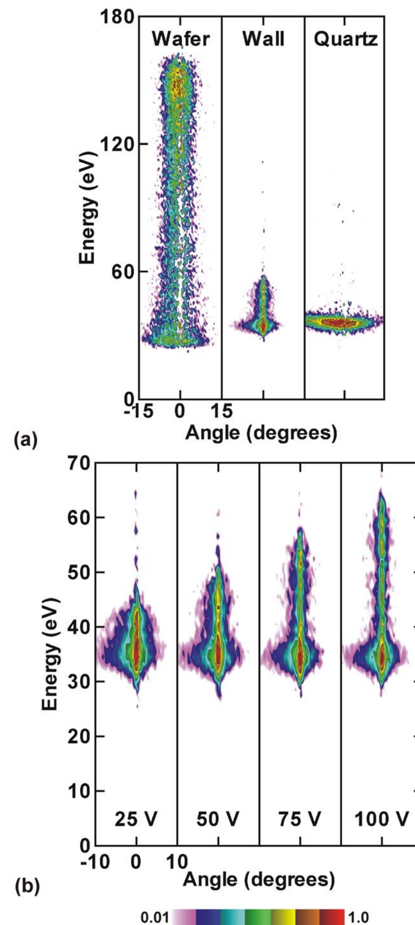

FIG. 4. IEADs summed over all ions for Ar/Cl_2=90/10, 500 W ICP, 15 mTorr, and 100 sccm. (a) Averaged over the wafer, wall, and quartz window for a 75 V substrate bias. (b) Averaged over the metal wall for biases of 25–100 V. The IEAD has a peak near the floating potential with a tail reflecting the positive excursion of the plasma potential. The plots are on a log scale plotted over 2 decades.

energy. The ion energies incident onto the metal sidewall and the quartz window peak at about 35 eV and are marginally above the threshold energies (30 eV) of surface reactions involving Si containing species. The probability for sputtering a $SiCl_2(s)$ site on the sidewall is 0.05 at 35 eV.

The shapes of the IEADs differ between the metal sidewall and the quartz window. The sheath at the electrically grounded metal sidewall oscillates with the amplitude of the plasma potential above ground. For example, the IEADs for all ions averaged over the metal wall are shown in Fig. 4(b) for rf biases of 25–100 V. For a 75 V rf bias and dc bias of −37 V, the plasma potential oscillates with an amplitude of about 38 V above ground but spends the majority of the rf period near the floating potential. As such, the IEAD has a peak near the floating potential (37 V) with a high energy tail reflecting the positive excursion of the plasma potential above the floating potential during the anodic part of the rf cycle. As the bias voltage increases, the plasma potential oscillates with a larger amplitude, thereby producing a tail to higher energies for the IEAD to the metal wall. However, since the floating potential is nearly independent of the rf bias, the low energy peak of the IEAD does not significantly vary. The IEAD is angularly broad at the lower energy of the floating potential and narrows in the higher energy tail produced by excursions of the plasma potential with increasing bias.

The IEAD incident on the quartz window has a single peak corresponding to the floating potential. The quartz, being a low capacitance dielectric, acts as an electrically floating body in contact with the plasma and so negatively charges to the floating potential with respect to the instantaneous plasma potential. The capacitance of the quartz is small enough that its charging to the floating potential is in near equilibrium with the oscillation of the plasma potential. As such, ions incident onto the quartz see a quasi-dc floating potential. The floating potential is largely determined by the electron and ion temperatures in the bulk plasma, each of which are weak functions of the rf bias which serves to dominantly accelerate ions into the substrate. As a result, the floating potential and the IEADs to the quartz window do not appreciably change with rf bias.

Results will first be discussed for the variant of the reaction mechanism where the $SiCl_2$ etch product does not stick to $SiCl_2(s)$ passivation on the walls. The coverages of $SiCl_x(s)$ on internal surfaces after processing a single wafer for 3 min are shown in Fig. 5(a) for rf biases of 25–100 V. The locations of the surfaces are shown in Fig. 2(a). (Note that the surface between 10.6 and 14.3 cm corresponds to the opening to the pump port.) As the bias voltage increases, the coverage of $SiCl_x(s)$ increases on all chamber surfaces except for the wafer. On the wafer, increasing the bias voltage increases the probability and rate of etching which reduces

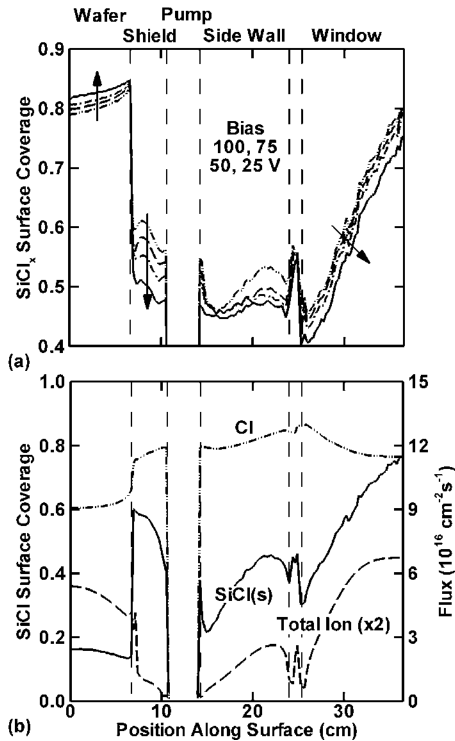

FIG. 5. Fractional surface coverages as a function of position along the surface after etching one wafer. (Reactor locations are shown in Fig. 2.) (a) Coverage of the sum of all $SiCl_x(s)$ for biases of 25–100 V. The arrows point in the direction of decreasing bias. As the bias increases, the coverage of $SiCl_x(s)$ increases on all surfaces except for the wafer. (b) Coverage of $SiCl(s)$ and fluxes of Cl and ions for a bias of 100 V. The variation in ion flux contributes to the variation in coverage of $SiCl(s)$.

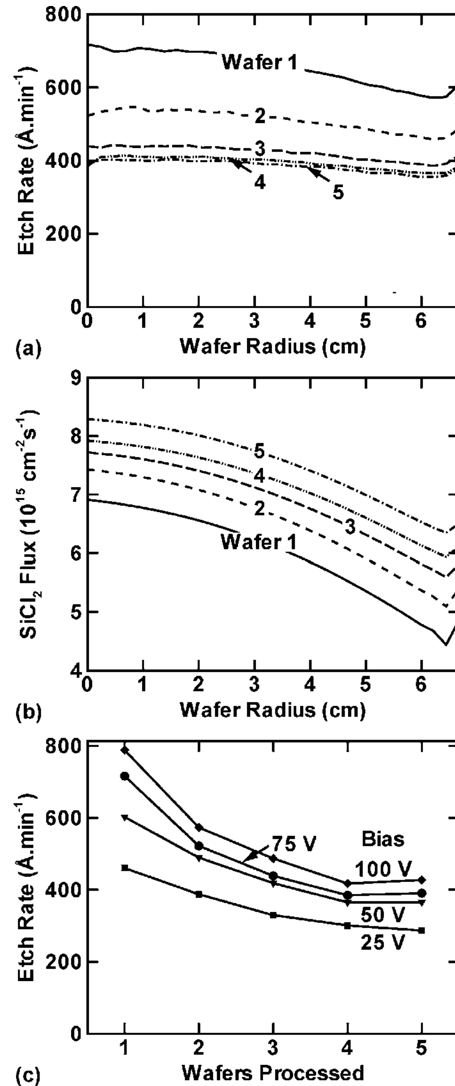

FIG. 6. Plasma and etch properties for sequential processing of five wafers in the same reactor. (a) Etch rate as a function of radius for a bias of 75 V. (b) Flux of etch product $SiCl_2$ to the wafer for a bias of 75 V. (c) Etch rate at the center of the wafer for biases of 25–100 V. Etch rates decrease with successive wafers due to the increase in formation of Si_2Cl_y etch blocks. Etch rates saturate by about the fifth wafer.

the residence time for a $SiCl_x(s)$ site before it is removed by etching. As such, at high bias voltages, the proportion of $SiCl_x(s)$ sites that are $SiCl(s)$ increases since the average degree of chlorination of any given site is lower. The $SiCl_x(s)$ coverage increases on nonwafer surfaces as the bias increases due to an increase in the total etch rate, producing larger fluxes of etch products, which deposit on the sidewalls as $SiCl_2(s)$. This increase occurs in spite of the increase in sputtering rates on the sidewalls produced by the higher energy tails to the IEADs [shown in Fig. 4(b)].

The coverage of $SiCl(s)$, and fluxes of Cl and sum of all ions on internal surfaces are shown in Fig. 5(b) for a rf bias of 100 V. The fluxes of Cl incident upon the nonwafer surfaces are uniform within about 10% resulting in a uniform Cl adsorption on these surfaces. Ion fluxes are largest to the quartz window due to the proximity of the ionization source directly under the antenna. With ion bombardment of the wafer, the $SiCl_2$ etch product deposits on sidewalls. Following subsequent sputtering of Cl from the $SiCl_2(s)$ sites, a coverage of $SiCl(s)$ is produced. The $SiCl_x(s)$ coverage on the walls increases with increasing bias because of the increase in production of etch produce in spite of the IEAD extending into a regime where $SiCl_2(s)$ begins to be sputtered to $SiCl(s)$. Nonwafer surfaces having higher ion fluxes but moderate energies have a higher surface coverage of $SiCl(s)$, such as on the quartz window. The $SiCl_x(s)$ coverage on the wafer decreases with increasing bias because the already high ion energies extend further into a regime of higher rates of sputtering of $SiCl_x(s)$ sites, which on the average leave more native Si sites. The nonuniform ion fluxes to nonwafer surfaces in large part contribute to the nonuniform coverage of $SiCl_x(s)$.

In the following discussion when radial dependencies are not shown, the surface coverages and etch rates for the wafer are at $l=0$ (center of the wafer) in Fig. 5(a). Results for the sidewall are for $l=19.5$ cm (midheight of the wall).

Etch rates at the end of a 180 s process as a function of position on the wafer for a rf bias of 75 V are shown in Fig. 6(a) for five wafers sequentially etched in the reactor undergoing seasoning. (Recall that each new wafer is devoid of etch products whereas the state of the reactor walls is retained from the previous etch.) On a wafer-to-wafer basis,

the etch rate decreases. The etch rate is center peaked for the first wafer as a consequence of the center-peaked ion flux. (The small scale variations in etch rate result from noise in the IEADs, derived from a Monte Carlo simulation, that are used to compute reaction probabilities.) The etch rates decrease with subsequent wafers after the first due, in large part, to the increase in the flux of $SiCl_2$ to the wafer, shown in Fig. 6(b), which produces $Si_2Cl_y(s)$ etch blocks. The etch rate decreases in spite of an increase in Cl flux. In this variant of the model, as the walls are passivated by etch products, the sticking probability for $SiCl_2$ decreases, thereby increasing its gas phase density and flux to the wafer. (Note that the subsequent removal of etch blocks does not contribute to the net etch rate.) The amount of the decrease in etch rate decreases for subsequent wafers, eventually saturating by about the fifth wafer when the reactor is fully seasoned. A coincidental synergy is that the radial uniformity of etching improves with wafer number as the larger flux of etch blocking $SiCl_2$ to the center of the wafer compensates for the higher ion fluxes.

This trend of decreasing etch rate occurs for all bias voltages. For example, etch rates for sequentially processed wafers for rf biases of 25–100 V are shown in Fig. 6(c). The change in etch rate between wafers 1 and 2 increases with increasing bias voltage, a consequence of the higher flux of etch products from and redepositing on the wafer. The etch rates eventually stabilize as a result of the wall coverages reaching a steady state. That is, the reactor becomes fully seasoned.

The coverages of silicon containing species after sequentially processing five wafers are shown in Fig. 7 for the wafer and in Fig. 8 for the metal walls for rf biases of 25–100 V. As additional wafers are etched, the fluxes of etch products to the wafer increases (as shown in Fig. 6) resulting in higher coverages of etch block species, $Si_2Cl_y(s)$. The etch blocks react with the surface sites occupied by $SiCl(s)$ and $SiCl_2(s)$ but not by $SiCl_3(s)$. For any wafer in the sequence, $SiCl_3$ coverage is largest at low biases as high bias voltages facilitate more rapid removal of higher chlorinated sites $[SiCl_2(s)$ and $SiCl_3(s)]$ resulting in a decrease of their coverage. Consequently, more native Si sites get chlorinated resulting in an increase of the coverage of $SiCl(s)$.

With an increasing number of processed wafers, the sidewalls are exposed to a larger total fluence of etch products, and so the total coverage of SiCl and $SiCl_2$ increases, as shown in Fig. 8. As the coverage of this passivation increases, the sticking coefficients for both etch products and Cl decrease. The higher etch rates at higher bias voltages increase the densities of $SiCl_2$ in the plasma and so produce larger fluxes of $SiCl_2$ to the walls. This produces more passivation which blocks the adsorption of Cl. These higher biases also produce larger excursions of the plasma potential which in turn produces higher ion energies to the walls. These higher ion energies enable sputtering of Cl from the $SiCl_2(s)$ sites, leaving $SiCl(s)$ passivation. The ratio of

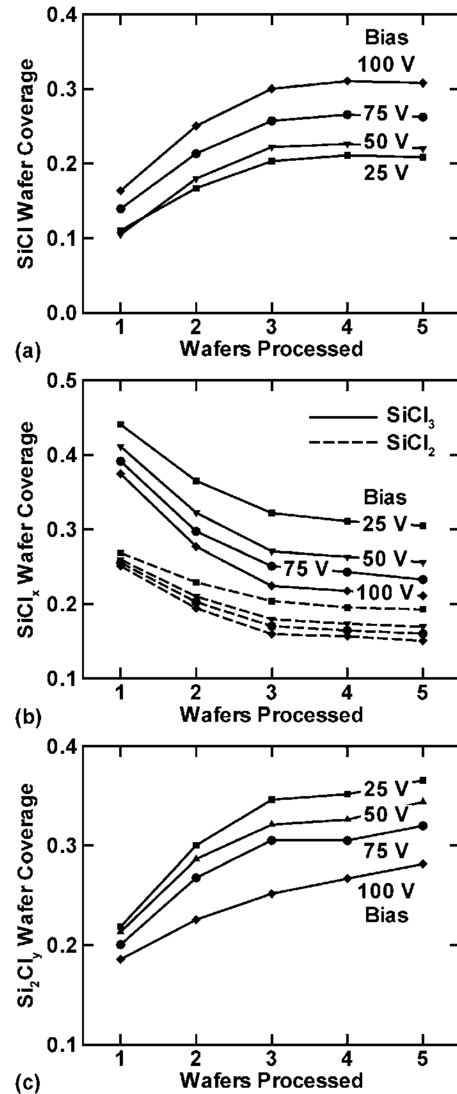

FIG. 7. Wafer surface coverages of silicon containing species for processing five wafers in the same reactor for different bias voltages. (a) SiCl, (b) $SiCl_2$ and $SiCl_3$, and (c) Si_2Cl_y. High bias voltages facilitate rapid removal of higher chlorinated sites on the wafer. As more wafers are processed the coverage of the etch blocks on the wafer increases, decreasing the etch rate.

$SiCl(s)$ to $SiCl_2(s)$ on the sidewalls depends on the relative probabilities of sputtering Cl, SiCl, or $SiCl_2$ from a $SiCl_2(s)$ site.

The surface coverages for the quartz window are shown in Fig. 9 after sequentially processing five wafers for a rf bias of 100 V. As more wafers are processed, the total flux and the gas phase density of etch products increases, and so the total coverage of $SiCl_2(s)$ increases. The ion energies incident on the quartz window peak at about 35 eV at which the probability of sputtering the $SiCl_2(s)$ is only about 0.05 and does not appreciably change with bias. Consequently, the change in the surface coverage of $SiCl(s)$ is not significant. As the surface coverage of the $SiCl_2(s)$ increases, the sticking coefficient for Cl decreases, thereby contributing to the decreasing surface coverage of Cl. With purely inductive coupling,

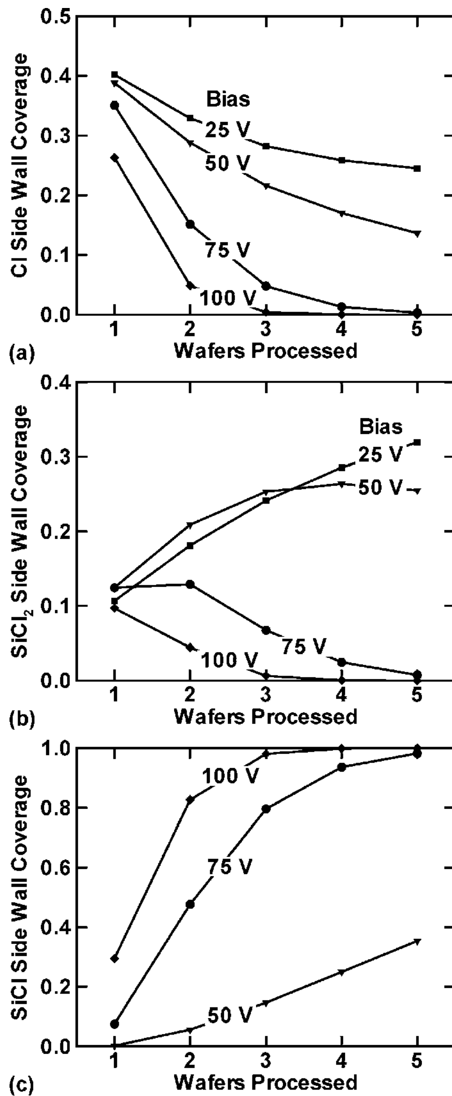

FIG. 8. Reactor wall surface coverages of silicon containing species for processing five wafers in the same reactor for different bias voltages. (a) Cl, (b) $SiCl_2$, and (c) SiCl. The Cl coverage decreases as more sites are passivated with $SiCl_x$. Larger biases produce higher ion energies which sputter Cl, leaving SiCl sites.

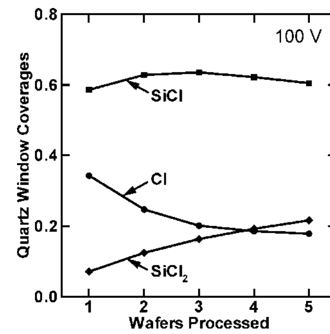

FIG. 9. Surface coverages of SiCl, $SiCl_2$, and Cl on the quartz window for processing five wafers in the same reactor for a bias of 100 V. As more wafers are processed, the total flux and the gas phase density of the etch products increases, increasing the total coverage of $SiCl_2$. The change in SiCl coverage is not significant due to the lower sputtering rates on the floating surface.

the quartz window has only a marginal effect on the gas phase densities since the ions incident onto the quartz see only a quasi-dc floating potential.

In the second variant of the reaction mechanism, $SiCl_2$ is allowed to continually stick to the sidewalls [Eq. (16)] and so buildup multiple layers of passivation. In this case, the walls will act as a continuous sink for the etch products (albeit with varying probability). The continuous consumption of etch product on the walls reduces the gas phase density of $SiCl_x$ and so decreases the flux of etch blocks back to the wafer. The more fully passivated walls decrease the sticking coefficients of Cl and so the flux of Cl to the wafer increases. The anticipated end result is an increase in etch rates.

Etch rates for sequentially processed wafers for a rf bias of 100 V are shown in Fig. 10(a) at the end of the 180 s process for the second variant of the reaction mechanism. The probability of reaction in Eq. (14) was varied from 0.6 to 0.9. The general trend when multiple layers are deposited on the reactor walls is for the etch rates to increase. The etch rates are, however, weakly dependent on the probability of deposition as the mechanism is not significantly affected by the thickness of the passivation layer. $SiCl_2$, continually depositing on the reactor walls, decreases the sticking coefficient of Cl which increases the flux of Cl while decreasing the flux of $SiCl_2$ to the wafer. The lower flux of $SiCl_2$ back to the wafer results in a lower surface coverage of etch blocks thereby increasing the etch rates.

The fluxes to the wafer of $SiCl_2$ and Cl^+ are shown in Fig. 10(b) for sequentially processed wafers. The flux of $SiCl_2$ does not significantly increase as more wafers are processed in the same chamber since once the walls are passivated their sticking coefficients are essentially constant. Increasing $SiCl_2$ sticking probability increases the thickness of the $SiCl_2(s)$ deposits on the sidewall, shown in Fig. 10(c), which tends toward a steady state after five wafers. The increase in etch rate with wafers processed results largely from the decrease in Cl sticking coefficient, and accompanying increase in Cl fluxes, and reduction in $SiCl_2$ fluxes to the wafer. The increase in Cl^+ flux relative to Cl_2^+, which more efficiently sputters etch blocks, also contributes to the increase in etch rates.

A subtle but important effect contributing to the increase in etch rate with the wafer processed is the role of the passivated walls as a virtual source of Cl. With the increase of wall passivation, ion bombardment of the sidewalls sputters Cl, particularly with high bias voltages which produce high energy tails to the IEADs to the walls. In a well seasoned reactor, the source of Cl from the walls can have a magnitude comparable to that by electron impact dissociation. This is particularly important to wafers after the first wafer where wall passivation releases Cl atoms stored from processing the previous wafer.

IV. COIL DESIGN AND SEASONING

The sputtering of the quartz window in ICP reactors resulting from capacitive coupling from the coil can be a

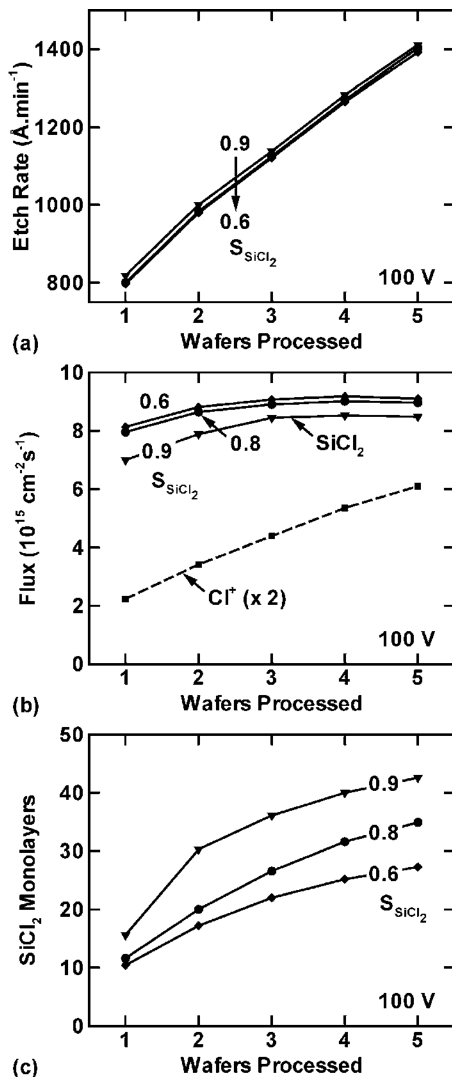

FIG. 10. Process properties for the variant of the reaction mechanism allowing multiple passivation layers on reactor walls. Results are for sequential processing of five wafers for a bias of 100 V while varying the $SiCl_2$ sticking probability. (a) Etch rate at the center of the wafer. (b) Flux of $SiCl_2$ and Cl^+ at the center of the wafer. (c) Layers of passivation on reactor walls. The etch rate increases when multiple layers of passivation are allowed on reactor walls due to the increase in Cl and Cl^+ fluxes and the decrease in $SiCl_2$ fluxes.

source of oxygen atoms which leads to deposition of silicon oxychloride films on the chamber walls.[43] To investigate these processes, capacitive coupling of the coils through the quartz window was included. Operationally, Poisson's equation for the electric potential is solved in the entire reactor domain (plasma, in materials and the air around the coils). Voltages on each turn of the coil obtained from a circuit model (or prior experience) are used as the potential boundary condition in solution of Poisson's equation. As quartz has a nonunity dielectric constant and negligible conductivity, it acts as a capacitor transmitting displacement current from the coil into conduction current in the plasma. Coil voltages of 300, 400, and 500 V at 10 MHz were applied to the inner, middle, and outer coils, for an antenna powered on the outside turn and terminated on the inner turn. Although Si is also sputtered from the quartz, to simplify the reaction mechanism, we allowed that only O atoms were sputtered.

The flux of O atoms sputtered from the quartz window is ultimately determined by the sheath voltage under the coils accelerating ions into the quartz. The sheath voltage in turn depends on the degree of capacitive coupling of the coils through the window. The amount of capacitive coupling can be controlled by the height of the coils above the quartz. Coils in contact with the quartz have the largest degree of coupling and so produce the largest sheath voltages. Lifting the coils off the window decreases the amount of capacitive coupling.

The IEADs incident on the quartz window averaged over the 0.8 cm centered under the coils are shown in Fig. 11. IEADs are shown for the coils in contact with the quartz (the standard configuration) and when the coils are displaced by about 0.4 cm above the quartz. The density and flux vectors of O atoms resulting from sputtering of the quartz for the standard configuration are shown in Fig. 12. For the standard configuration, the IEADs under the outer coil extend to energies above the threshold for sputtering. The IEADs are only marginally above the threshold under the middle coil. Below the inner coil, the IEADs differ little from those on floating surfaces. With the coils raised above the quartz window, there is less capacitive coupling and smaller sheath potentials under the coils. As a result, the IEADs under the coils have lower energies, with the threshold for sputtering being exceeded only under the outer coil. Sputtering of O atoms occurs dominantly under outer coil in both cases, producing a peak density of 7×10^{11} cm^{-3} near their source for the standard configuration. The source of O atoms is dominantly the quartz window with a secondary source coming from the wafer due to sputtering of etch blocks. (Note that the flux vectors in Fig. 12 show only direction and not magnitude.)

The fluxes of O and O^+ to the wafer resulting from sputtering are shown in Fig. 11(c). The flux of O^+ is two orders of magnitude lower (2.2×10^{13} cm^{-2} s^{-1}) than the fluxes of the majority ions, Ar^+ and Cl^+, and so does not play a significant role in the reaction kinetics. The flux of O (3.9 $\times10^{15}$ cm^{-2} s^{-1}) is comparable to that of the etch products and of sufficient magnitude to affect the etch rates. The lower ion energies when coils are displaced sputter fewer O atoms, and so the fluxes of O and O^+ to the wafer decrease by about 50%.

O atoms to the wafer adsorb on the chlorinated silicon sites forming silicon oxychloride (SiOCl) which is an etch block. For example, the coverages of silicon containing species on the wafer after etching one wafer are shown in Fig. 13 for biases of 25–100 V. Since the sputtering of the quartz window is the only source of oxygen, the flux of oxygen atoms to the wafer does not significantly change with bias voltage. At low bias voltages, ion energies are not high enough to remove the etch block and so the coverage of SiOCl(*s*) is high. As the bias increases, the rate of removal of SiOCl(*s*) increases, thereby removing the etch block and enabling the etch to proceed. The increase in coverage of

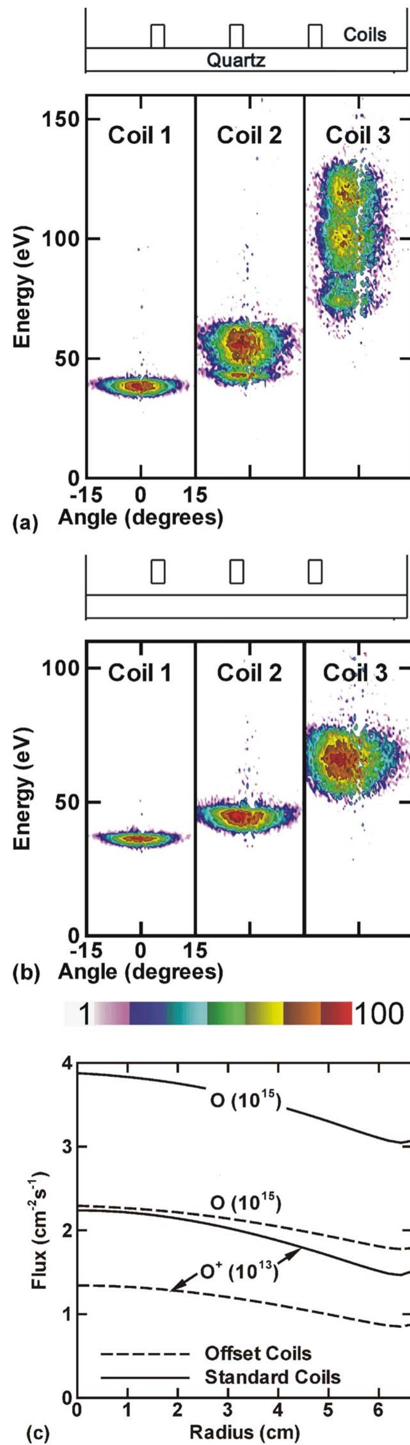

FIG. 11. Plasma properties for different coil configurations for Ar/Cl_2 =90/10, 500 W ICP, 15 mTorr, 100 sccm, and 75 V substrate bias. (a) IEADs on the quartz under different turns of the antenna with the coils directly on the quartz. (b) IEADs for coils offset by 0.4 cm which reduces the amount of capacitive coupling lowering the ion energies. (c) O and O^+ fluxes to the wafer as a function of radius for the two coil configurations. The flux of O atoms is comparable to that of the etch products. IEADs are shown in a log scale plotted over 2 decades.

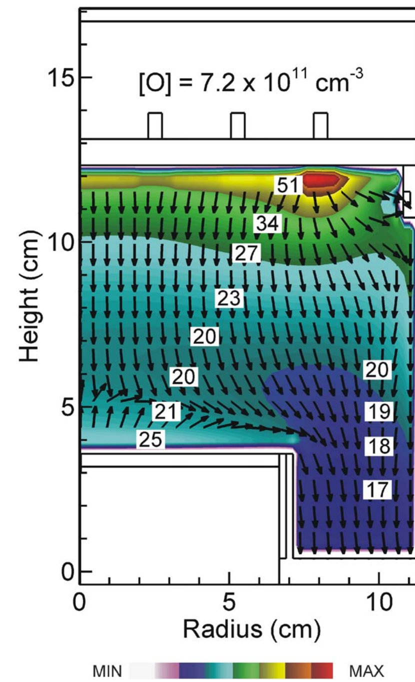

FIG. 12. Density of oxygen atoms sputtered with the coils set on the quartz window. The flux vectors show only direction and not magnitude. The peak density is below the outer turn of the coil where the capacitive coupling is maximum. The contour labels are percentages of the maximum density shown in the figure.

SiCl(*s*) with increasing bias voltage results from at least two effects. At high biases, the higher chlorinated sites are etched more rapidly exposing native Si sites which get chlorinated as SiCl(*s*). Further, the etch block SiOCl(*s*) is eliminated by removing the adsorbed oxygen, leaving SiCl(*s*). This latter trend results from our particular surface model in which sputtering of the etch block preferentially removes O as opposed to Cl. Preferential sputtering of Cl would retain the site as an etch block and so require a second sputtering event to enable etching to proceed. This would intensify the etch blocking nature of the sputtered oxygen.

The oxygen sputtered from the quartz window and from the wafer also adsorb on the sidewalls. The IEADs incident on the sidewalls, though having a high energy tail, peak at about 35 eV and so ion fluxes do not efficiently remove SiOCl(*s*) which ultimately saturate the surface. The coverage of SiOCl(*s*) on the quartz is generally lower due to the higher

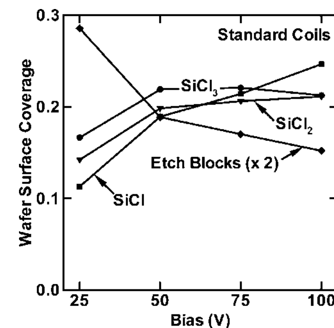

FIG. 13. Surface coverages of silicon containing species and etch blocks on the wafer after etching one wafer for bias of 25–100 V. High bias voltages enable high ion energies to sputter etch blocks on the wafer, decreasing their coverage.

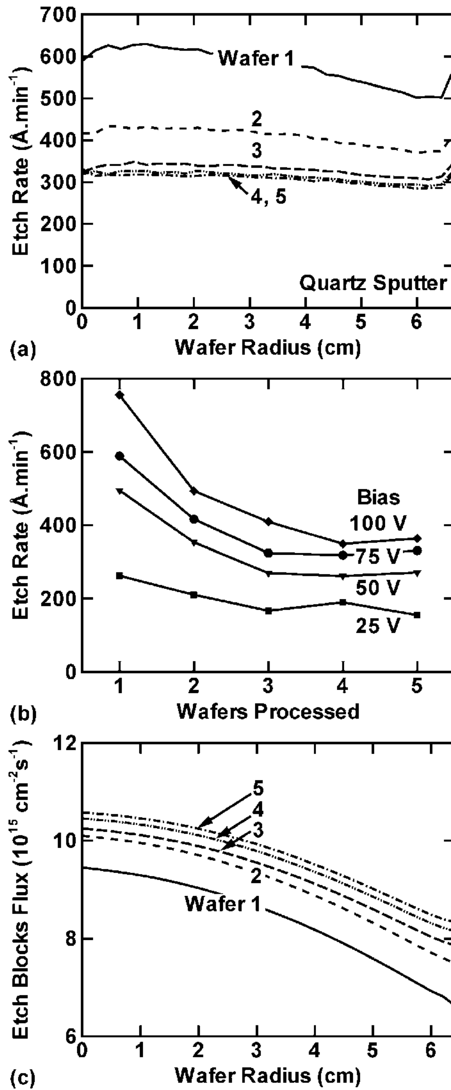

FIG. 14. Plasma properties and etch rates for sequential processing of five wafers in the same reactor when oxygen is sputtered from the quartz window. (a) Etch rates as a function of radius for a bias of 75 V. (b) Etch rate at the center of the wafer for biases of 25–100 V. (c) Flux of etch block forming species. Etch rates decrease with successive wafers due to the increasing surface coverage of SiOCl and Si_2Cl_y etch blocks.

rates of sputtering due to the capacitive coupling. Consequently, with processing successive wafers, the density of etch products in the bulk plasma increases with bias voltage. This partially offsets an increase in etch rate which would otherwise result from removing etch blocks on the wafer.

Etch rates as a function of radius for a bias of 75 V are shown in Fig. 14(a) for sequential etching of five wafers in a seasoning reactor with sputtering of the quartz. Etch rates for the first wafer peak at the center of the wafer. With processing of successive wafers, the etch rate decreases and the uniformity improves. The decrease in etch rates occurs for all biases, as shown in Fig. 14(b). The etch rates eventually stabilize as a result of the balance between the flux of etch block forming species (O and $SiCl_2$) and the flux of etching species (ions). The improvement in uniformity with additional wafers is due to the increase in fluxes of etch block forming species, O and $SiCl_2$, as shown in Fig. 14(c), which have a maximum on axis. When new wafers are etched in a progressively seasoned reactor, the etch products from that wafer are not deposited on the reactor wall that is saturated with SiOCl(s). $SiCl_2$ therefore redeposits on the wafer as $Si_2Cl_y(s)$, forming the etch block. The higher flux of etch blocks at the center of the wafer decreases the etch rate more rapidly than at outer radii, thereby balancing the center peaked ion flux and providing a more uniform etch.

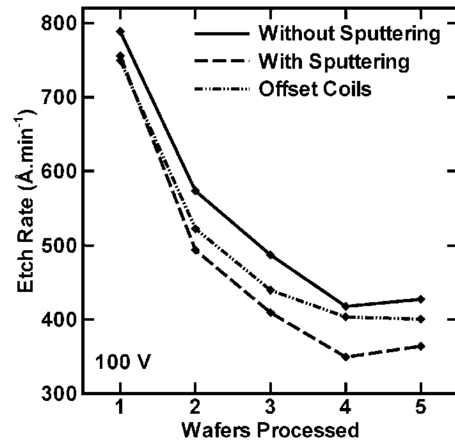

FIG. 15. Effect of capacitive coil coupling for sequential processing of five wafers for a 100 V bias. Oxygen sputtered from the quartz window increases coverage of etch block species, reducing etch rates. Capacitive coupling is reduced by offsetting the coils above the dielectric window which reduces sputtering rates.

The importance of reactor design and maintaining critical dimensions in construction of the reactor are illustrated by the etch rates shown in Fig. 15 (for a rf bias of 100 V). Etch rates are plotted at the center of the wafer as a function of wafer number for different coil configurations. Etch rates are uniformly higher in the absence of capacitive coupling, as might be obtained with a Faraday shield. With the coils set directly on the quartz window, the capacitive coupling is maximum and the sputtering of O atoms is greatest. This configuration results in the largest production of etch blocks and the lowest etch rates. Offsetting the coils from the quartz window reduces the capacitive coupling while decreasing the sputtering of O atoms and produces intermediate etch rates. Displacement of the coils by only a few millimeters, as might occur during preventative maintenance of the reactor, could have a measurable effect on etch rates due to the change in capacitive coupling and sputtering rates of the window.

V. REAL-TIME AND RUN-TO-RUN CONTROL STRATEGIES

To mitigate process drifts, cleaning and conditioning steps are often employed between production wafers to ensure that the initial conditions of the reactor are the same for each wafer. These drifts can occur while processing a single wafer as well as on a wafer-to-wafer basis. Real time control (RTC) and wafer-to-wafer control are therefore both options to maintain uniform etch rates. The choice of the sensor-

actuator pair (or pairs) is largely governed by the ability to measure the desired properties and to correlate an actuator setting with a desired change in reactive fluxes. In this study, we chose the etch rate as the sensor, as might be measured by a multicolor interferometer, and the bias voltage as the actuator. In the parameter space of interest, the etch rate is nearly a monotonic function of the bias voltage and so allows for a simple control scheme. The disadvantages to varying voltage are the possibility of compromising selectivity or etch profile. These effects will be addressed in a subsequent study. A simple proportional control algorithm was used to adjust the bias voltage to maintain a constant etch rate.

The computational strategy to investigate control schemes is as follows. The RTC aspect of the control is obtained by specifying an etch rate as the set point. Changes in the etch rate from the set point are treated as perturbations. Sensor measurements and actuator adjustments are made at intervals of approximately 7–8 s (referred to as controller time steps, T). The proportional controller resets the bias to obtain the set point etch rate using a gain of 0.3. When a new wafer is placed into a seasoned reactor, the bias voltage (actuator) is set to the value the RTC scheme specified at the end of the prior wafer that was processed. This constitutes the run-to-run aspect of control.

Etch rates are shown in Fig. 16(a) for a default (initial) rf bias of 75 V for five wafers with and without control. The bias voltage (actuator) with control is also shown. These results are for the first variant of the reaction mechanism where passivation on reactor walls is limited to a single layer. In the absence of control, the etch rate decreases as wafers are processed due to the redeposition of etch products. During a single process, the etch rate of the initially clean wafer decreases as etch products build on the wafer surface and then tends toward a steady state. The initial etch rate is lower when a new wafer is processed as a result of the previously deposited etch products on the walls decreasing $SiCl_2$ sticking coefficients and increasing the $SiCl_2$ flux to the wafer, which increases the etch block coverage.

The control scheme is implemented at $T=3$ to maintain the etch rate at its set point, in this case the etch rate at controller time $T=1$ of the first wafer. For each successive wafer processed, the etch rate is restored by $T=6$. During etching of the first wafer, the bias voltage generally increases to sputter the redeposition products to maintain the etch rate. The actuator voltage is at its maximum at the end of the process. When the second, clean wafer begins to be etched, the initial actuator voltage (corresponding to the previous wafer covered with etch blocks) exceeds that required to achieve the set point etch rate. In response to the higher etch rate, the bias voltage (actuator) is lowered in about $\Delta T=4$ to nearly the default value. As the wafer is further processed and the redeposition fluxes increase, which would otherwise decrease the etch rate, the controller increases the bias voltage. On a run-to-run basis after the second wafer, the ending bias voltage is higher than for the prior wafer.

Etch rates for five sequential wafers with and without control, and actuator voltage, for a default (initial) bias of 100 V are shown in Fig. 16(b). The reaction mechanism is the second variant where multiple layers of passivation build on the walls. In absence of control, the etch rate increases as wafers are processed as the reactor walls act as a sink for the $SiCl_2$ etch product thereby decreasing the flux of etch products to the wafer. During a single process, the etch rate increases most rapidly early during the process prior to achieving a near steady state. The initial etch rate is higher when a new wafer is processed as a result of the adsorbed etch product which decreases the sticking coefficient of Cl and thus increases the flux of Cl and Cl^+ to the wafer which results in a higher etch rate.

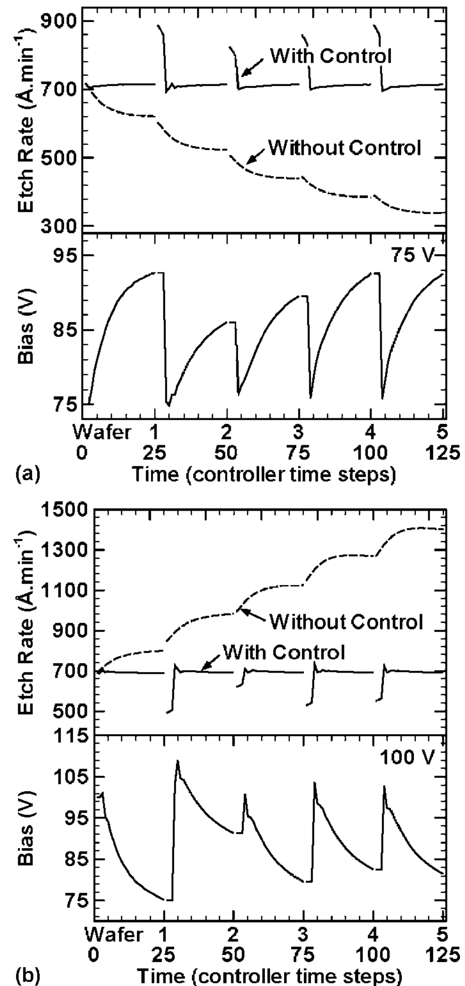

FIG. 16. Sensor (etch rate) and actuator (voltage) time history for real-time and run-to-run control for sequential processing of five wafers in a seasoning reactor. (a) Reaction mechanism where only a single layer of passivation is permitted. The general trend is to increase the bias voltage to enable sputtering of the redeposition products. (b) Reaction mechanism where multiple layers of passivation are permitted. The general trend is to decrease the bias voltage to offset the increasing etch rates.

The control scheme is implemented at $T=3$ of the first wafer to maintain the etch rate at its set point (etch rate at $T=1$). In general, the bias voltage is decreased to offset the increasing flux of Cl^+ to the wafer. Retaining the bias voltage from the previous run results in a lower initial etch rate, prompting the controller to increase the bias voltage. As the

Cl and Cl^+ fluxes increase during the process, which would otherwise increase the etch rates, the actuator voltage is decreased to maintain the set point etch rate.

The just discussed control scheme works well when the etch is in an ion limited regime and etch rates can be uniformly increased with increasing bias voltage. We found that achieving control at higher biases is more complex due to a transition from an ion limited regime to a neutral limited regime. That is, the etch rate is limited more by the availability of Cl flux than by ion flux (or energy). In these regimes, a two point control scheme is likely required to control both ion and Cl fluxes.

VI. CONCLUDING REMARKS

Plasma-surface interactions were modeled to investigate the seasoning of reactors during etching of *p*-Si in Ar/Cl_2 inductively coupled plasmas. When etch products have a finite rate of deposition on sidewalls, etch rates decreased both during a single process and on a wafer-to-wafer basis as the chamber was seasoned. The decrease in the etch rate was due to the increase in fluxes of etch blocking species to the wafer. In a mechanism where etch products continually stick to walls, enabling Cl atom fluxes to increase without there being an increase in etch blocking species, the etch rates increased both during a process and wafer-to-wafer. Capacitive coupling from the coils through the quartz window can lead to sputtering of oxygen atoms which, for this particular chemistry, results in the formation of silicon oxychloride films, an etch block which leads to lower etch rates. The capacitive coupling through the coils can be mitigated by changes in the placement of the coils above the quartz window. To combat the drift in process rates resulting from seasoning, a feedback control algorithm was implemented. Real-time and run-to-run control was achieved using a proportional controller with etch rate as a sensor and bias voltage as an actuator.

ACKNOWLEDGMENTS

This work was supported by Semiconductor Research Corporation, Applied Materials, Freescale, and National Science Foundation (Grant No. CTS05-20368). The authors particularly thank Peter L.G. Ventzek, Shahid Rauf, and Phillip J. Stout for their guidance during this investigation.

[1]L. Stafford, J. Margot, S. Delprat, M. Chaker, and S. J. Pearton, J. Appl. Phys. **101**, 083303 (2007).
[2]O. Joubert, E. Pargon, X. Detter, T. Chevolleau, G. Cunge, and L. Vallier, in *Proceedings of the 8th International Symposium on Plasma and Process Induced Damage*, April 2003, pp. 12–15.
[3]M. Kogelschatz, G. Cunge, O. Joubert, L. Vallier, and N. Sadeghi, Contrib. Plasma Phys. **44**, 413 (2004).
[4]S. Xu, Z. Sun, X. Qian, J. Holland, and D. Podlesnik, J. Vac. Sci. Technol. B **19**, 166 (2001).
[5]G. Cunge, O. Joubert, and N. Sadeghi, J. Appl. Phys. **94**, 6285 (2003).
[6]E. A. Joseph, B. Zhou, S. P. Sant, L. J. Overzet, and M. J. Goeckner, J. Vac. Sci. Technol. A **22**, 689 (2004).
[7]B. Zhou, E. A. Joseph, S. P. Sant, Y. Liu, A. Radhakrishnan, L. J. Overzet, and M. J. Goeckner, J. Vac. Sci. Technol. A **23**, 1657 (2005).
[8]S. J. Ullal, T. W. Kim, V. Vahedi, and E. S. Aydil, J. Vac. Sci. Technol. A **21**, 589 (2003).
[9]T. W. Kim and E. S. Aydil, J. Electrochem. Soc. **150**, G418 (2003).
[10]S. Xu, Z. Sun, A. Chen, X. Qian, and D. Podlesnik, J. Vac. Sci. Technol. A **19**, 871 (2001).
[11]O. Joubert, G. Cunge, B. Pelissier, L. Vallier, M. Kogelschatz, and E. Pargon, J. Vac. Sci. Technol. A **22**, 553 (2004).
[12]S. J. Ullal, H. Singh, J. Daugherty, V. Vahedi, and E. S. Aydil, J. Vac. Sci. Technol. A **20**, 1195 (2002).
[13]R. Ramos, G. Cunge, O. Joubert, N. Sadeghi, M. Mori, and L. Vallier, Thin Solid Films **515**, 4846 (2007).
[14]V. C. Venugopal, A. J. Perry, K. V. Wallace, and D. J. Cooperberg, Proc. SPIE **5188**, 200 (2003).
[15]V. C. Venugopal and A. J. Perry, Proc. SPIE **4779**, 98 (2002).
[16]T. E. Benson *et al.*, J. Vac. Sci. Technol. B **14**, 483 (1996).
[17]M. Sarfaty, C. Baum, M. Harper, N. Hershkowitz, and J. L. Shohet, Jpn. J. Appl. Phys., Part 1 **37**, 2381 (1998).
[18]J. Y. Choe, I. P. Herman, and V. M. Donnelly, J. Vac. Sci. Technol. A **15**, 3024 (1997).
[19]R. Patrick, S. Baldwin, and N. Williams, J. Vac. Sci. Technol. A **18**, 405 (2000).
[20]C. Lin, K.-C. Leou, and K.-M. Shiao, J. Vac. Sci. Technol. A **23**, 281 (2005).
[21]V. M. Donnelly, J. Vac. Sci. Technol. A **14**, 1076 (1996).
[22]C. Garvin, D. S. Grimard, and J. W. Grizzle, J. Vac. Sci. Technol. A **17**, 1377 (1999).
[23]T. E. Benson, A. Ramamoorthy, L. I. Kamlet, and F. L. Terry, Thin Solid Films **313–314**, 435 (1998).
[24]M. Sarfaty, C. Baum, M. Harper, N. Hershkowitz, and J. L. Shohet, Plasma Sources Sci. Technol. **7**, 581 (1998).
[25]W. Z. Collison, T. Q. Ni, and M. S. Barnes, J. Vac. Sci. Technol. A **16**, 100 (1998).
[26]N. V. Mantzaris, A. Boudouvis, and E. Gogolides, J. Appl. Phys. **77**, 6169 (1995).
[27]E. Meeks, R. S. Larson, S. R. Vosen, and J. W. Shon, J. Electrochem. Soc. **144**, 357 (1997).
[28]B. A. Helmer and D. B. Graves, J. Vac. Sci. Technol. A **16**, 3502 (1998).
[29]D. Zhang and M. J. Kushner, J. Vac. Sci. Technol. A **19**, 524 (2001).
[30]V. Vyas and M. J. Kushner, J. Vac. Sci. Technol. A **24**, 1955 (2006).
[31]C. F. Abrams and D. B. Graves, J. Appl. Phys. **86**, 2263 (1999).
[32]P. Subramonium and M. J. Kushner, J. Vac. Sci. Technol. A **20**, 325 (2002).
[33]C. C. Cheng, K. V. Guinn, V. M. Donnelly, and I. P. Herman, J. Vac. Sci. Technol. A **12**, 2630 (1994).
[34]E. Meeks and J. W. Shon, IEEE Trans. Plasma Sci. **23**, 539 (1995); E. Meeks and J. W. Shon (private communication).
[35]R. J. Hoekstra, M. J. Grapperhaus, and M. J. Kushner, J. Vac. Sci. Technol. A **15**, 1913 (1997).
[36]G. Cunge, M. Kogelschatz, O. Joubert, and N. Sadeghi, Plasma Sources Sci. Technol. **14**, S42 (2005).
[37]S. J. Ullal, H. Singh, V. Vahedi, and E. S. Aydil, J. Vac. Sci. Technol. A **20**, 499 (2002).
[38]S. J. Ullal, A. R. Godfrey, E. Edelberg, L. Braly, V. Vahedi, and E. S. Aydil, J. Vac. Sci. Technol. A **20**, 43 (2002).
[39]S. J. Ullal, H. Singh, J. Daugherty, V. Vahedi, and E. S. Aydil, J. Vac. Sci. Technol. A **20**, 1939 (2002).
[40]M. J. Grapperhaus, Z. Krivokapic, and M. J. Kushner, J. Appl. Phys. **83**, 35 (1998).
[41]D. S. Stafford and M. J. Kushner, J. Appl. Phys. **96**, 2451 (2004).
[42]S. Rauf and M. J. Kushner, IEEE Trans. Semiconductor Manuf. **11**, 486 (1998).
[43]M. Kogelschatz, G. Cunge, and N. Sadeghi, J. Vac. Sci. Technol. A **22**, 624 (2004).